INVERTED PENDULUM STUDIES FOR SEISMIC ATTENUATION

California Institute of Technology
SURF Final Report 2005

LIGO Caltech

Supervisor: Dr. Riccardo De Salvo
Mentor: Dr. Calum I. Torrie

Ilaria Taurasi

University of Sannio at Benevento, Italy

LIGO T060048-00-R

1. Introduction to LIGO

The Laser Interferometer Gravitational Wave Observatory (LIGO) is an international collaboration of scientist and engineers working together in the search for gravitational waves. Gravitational waves are ripples in space-time emitted by super-dense objects in space, such as black holes and binary stars. They have been predicted by Einstein and proved indirectly, through the accurate measurement of the orbital damping of a binary pulsar [1], but the goal is that the LIGO project, along with its counterparts around the world, will finally prove their existence directly by observing their effect on freely falling test masses. LIGO currently has facilities on two sites in Hanford, Washington (see Figure 1.1), and Livingston, Louisiana, with which gravitational waves will be measured.

Figure 1.1: LIGO Hanford Site

Potential changes and upgrades to the current facilities are conceived, designed, and tested at the California Institute of Technology (Caltech), the Massachusetts Institute of Technology (MIT), and the GEO 600 German-British Collaboration.

LIGO will use an approach known as interferometry to achieve his goal. Light from a laser beam enters the two arms of a Michelson interferometer [2] at right angles to each other, and the setup will be able to measure differential changes in the length of the arms due to (quadrupole) gravitational waves, as shown in Figure 1.2.

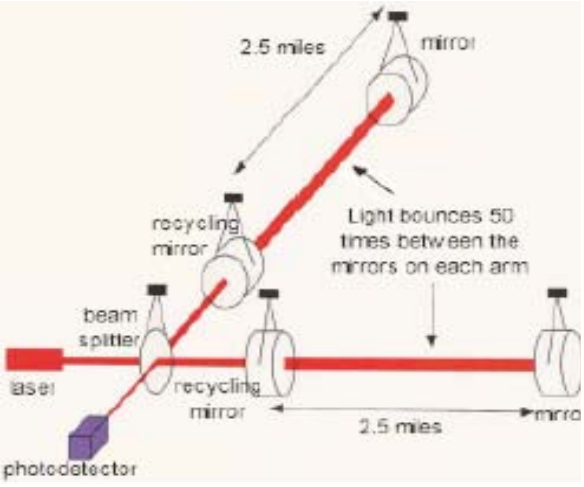

Figure 1.2: LIGO Interferometer

If there is any change in the length of the arm, a change in the light intensity will be detected by a photodetector. However, the expected change is so small that it will be nearly impossible to detect without filtering out noise of photon, thermal, and seismic origin. Advanced LIGO will incorporate new designs to reduce each one of these to acceptable values.

2. Seismic noise and the role of the Inverted Pendulum

Seismic noise is an unavoidable noise source for interferometers built on Earth. It is excited by natural phenomena like macro-seismic, oceanic, and atmospheric activities, as well as by human activities [3]. The unwanted and unpredictable (random) signal of an interferometer, caused by continuous and sporadic ground motion, is named "seismic noise". The ground motion transmits to the motion of the test masses through different paths. The most straightforward path is that the horizontal ground motion at the suspension point of the test mass causes the longitudinal motion of the test mass. Ground noise was measured at the LIGO Livingston site by A. Rohay from October 26 to November 3, in 1995 [4]. The seismometers used for these measurements give accurate ground noise readings from 0.1-50 Hz and give an upper bound on seismic motion above 50 Hz. The data exhibit a large peak between 0.1-0.3 Hz, which is the so-called microseismic peak, caused by ocean-wave activity.

The seismic spectrum of the earth generally shows increasing power towards low frequencies. There are two characteristic features that cause large motions over small frequency bands. These are the earth tides near 10^{-5} Hz and a microseismic peak near 0.15 Hz. The earth tides are a coherent background driven by the motions of the sun and moon with diurnal and semidiurnal periods. The microseismic motion noise is described by a peak in the power spectrum whose width and frequency are comparable [5]. The microseismic motion occurs at a

frequency below the resonant frequencies of most laboratory apparatus. Thus for any apparatus whose physical size is much less than a kilometer, the relative motion resulting from microseismic excitation is largely common mode and hence often goes unnoticed. The 40-meter interferometer, for example, is relatively immune to the effects of microseismic excitation and also earth tides. For interferometers with baselines of order several kilometers, the largest random contribution to the relative motions of mirrors in the arms can arise from the microseismic excitation. A considerable simplification occurs if we choose a non-inertial frame for this situation. Since most of the interferometer optics (with the exception of the end mirrors) are contained in a corner building with 100m sides. This building and its optics probably respond to the microseism like a rigid body.

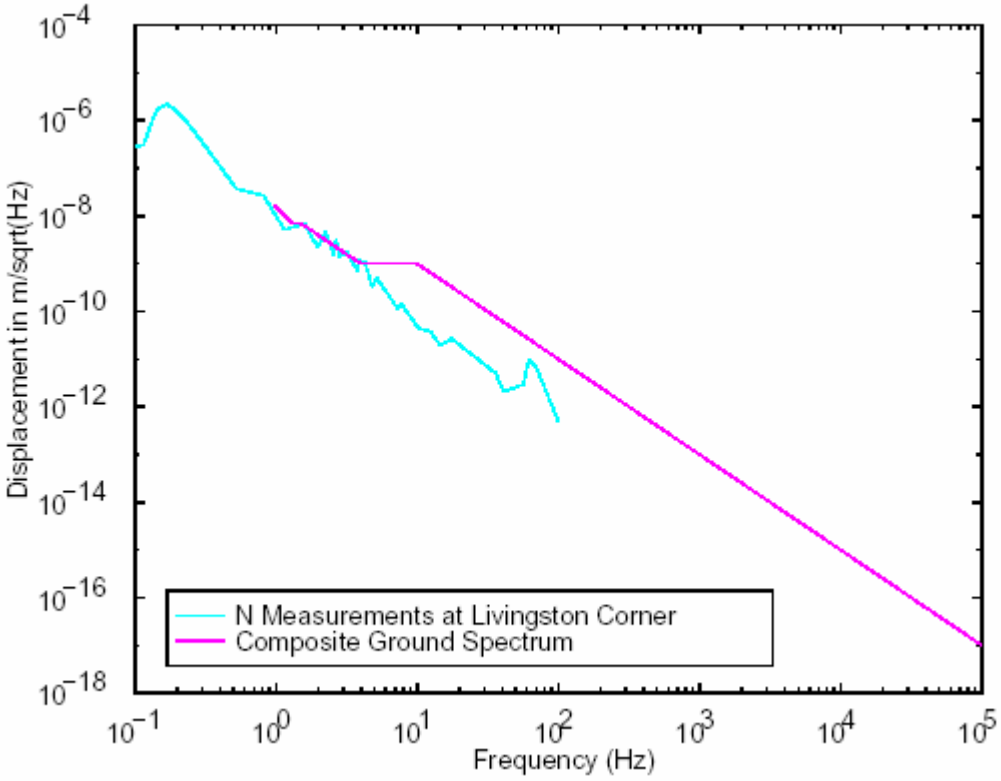

Figure 1.3: Ground noise spectrum measured at the Livingston, Louisiana site.

Since the peak ground motion is of the order of 10^{-6} m, as shown in Figure 1.3, and the expected GW signal is 10^{-18} m, we need attenuation factors of the order of 10^{-12}. In order to obtain an adequate bandwidth, especially at low frequency (~10 Hz), the residual seismic

noise acting on the optics needs to be further attenuated within the expected band of the sought signals.

2.1 The Inverted Pendulum: basic principles

An Inverted Pendulum (shortly IP) is a mechanical harmonic oscillator whose peculiarity is to make possible to obtain a very low resonant frequency, typically 30 mHz, for horizontal oscillations[6]. In fact, using the restoring torque of a flex joint, to balance the torque due to the gravity force (see Figure 2.1), an inverted pendulum with a leg of 1m can be tuned to reach a resonant frequency below 100mHz. The IP is implemented in the LIGO Seismic Attenuation System (SAS) to achieve three main objectives:

- to guarantee sufficient attenuation at frequencies extending down to the micro-seismic peak
- to realize a mean to position the entire system without requiring large forces
- to implement a quasi-inertial stage on which to detect the recoil and actively damp the motion of the suspended chain.

To achieve these aims, the IP is implemented using an elastic-flex joint counteracted by a gravitational anti-spring. To understand the basic dynamics of an inverted pendulum let us think of a simple ideal model, sketched in Figure 2.1: a load of mass M is supported by a massless rigid vertical rod of length l connected to ground by means of an elastic joint of angular stiffness κ [6]. Let θ be the angle between the rod and the vertical.

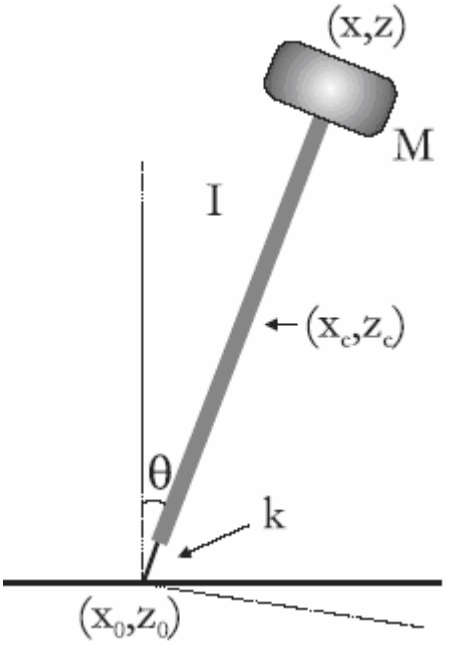

Figure 2.1: Schematic model of the inverted pendulum

The equation of motion is:

$$I\ddot{\theta} = -\kappa\theta + Mgl\sin\theta \tag{2.1}$$

where I is the moment of inertia of the system with respect to the suspension point O, identified by the coordinates x_0, z_0, $N_{el} = -k\vartheta$ is the elastic torque and $N_{grav} = Mgl \cdot \sin\vartheta$ is the gravity torque. In the small angle approximation (2.1) is written:

$$I\ddot{\theta} = -\kappa_{\text{eff}}\theta \tag{2.2}$$

where

$$\kappa_{\text{eff}} = \kappa - Mgl \tag{2.3}$$

is the *effective spring constant*: the gravity acts as an antispring, reducing the overall stiffness. The physics of the system is well described in terms of the potential energy:

$$U_{\text{pot}} = \frac{1}{2}\kappa\theta^2 + Mgl(\cos\theta - 1) \simeq \frac{1}{2}\kappa_{\text{eff}}\theta^2 + Mgl\frac{\theta^4}{4!} + O(\theta^6) \tag{2.4}$$

In the small angle approximation and for $\kappa > 0$ the quadratic term in (2.4) dominates and the system is a simple oscillator. By reducing the value of κ the potential "flattens" around $\theta = 0$

and this corresponds to small restoring force and small resonant frequency. When $k_{eff} \approx 0$ the quartic term dominates at small angles (see Figure 2.2).

When the gravity starts dominating ($k_{eff} < 0$) θ =0 is no more a point of stable equilibrium:

U(θ) has instead two minima at

$$\theta = \pm\sqrt{12\frac{-\kappa_{\text{eff}}}{Mgl}} \tag{2.5}$$

When $k_{eff} > 0$ the potential is always negative and the system is unstable.

In the following, rather than using the angle θ, we shall refer to the IP linear displacement x measured at the top ($x = l\theta$) of the rod and to the linear stiffness. The equation of motion for a (small) displacements x is:

$$M\ddot{x} = -(k - \frac{Mg}{l})x + O(x^3) = \tilde{k}x + O(x^3) \tag{2.6}$$

In Figure 2.2 the reduced potential energy *Upot/k* is plotted versus the angle θ for different values of the gravity-elastic ratio $R = Mgl/k$.

For $R << 1$ the system is far from instability, but the force dependence on θ is steep;

for $R < 1$ the IP is still stable and a low frequency is achieved;

for $R = 1$the restoring force around $\theta=0$ is null;

for $R < 1$ the system becomes bi-stable;

for $R>>1$ there is not any equilibrium position and the IP collapses.

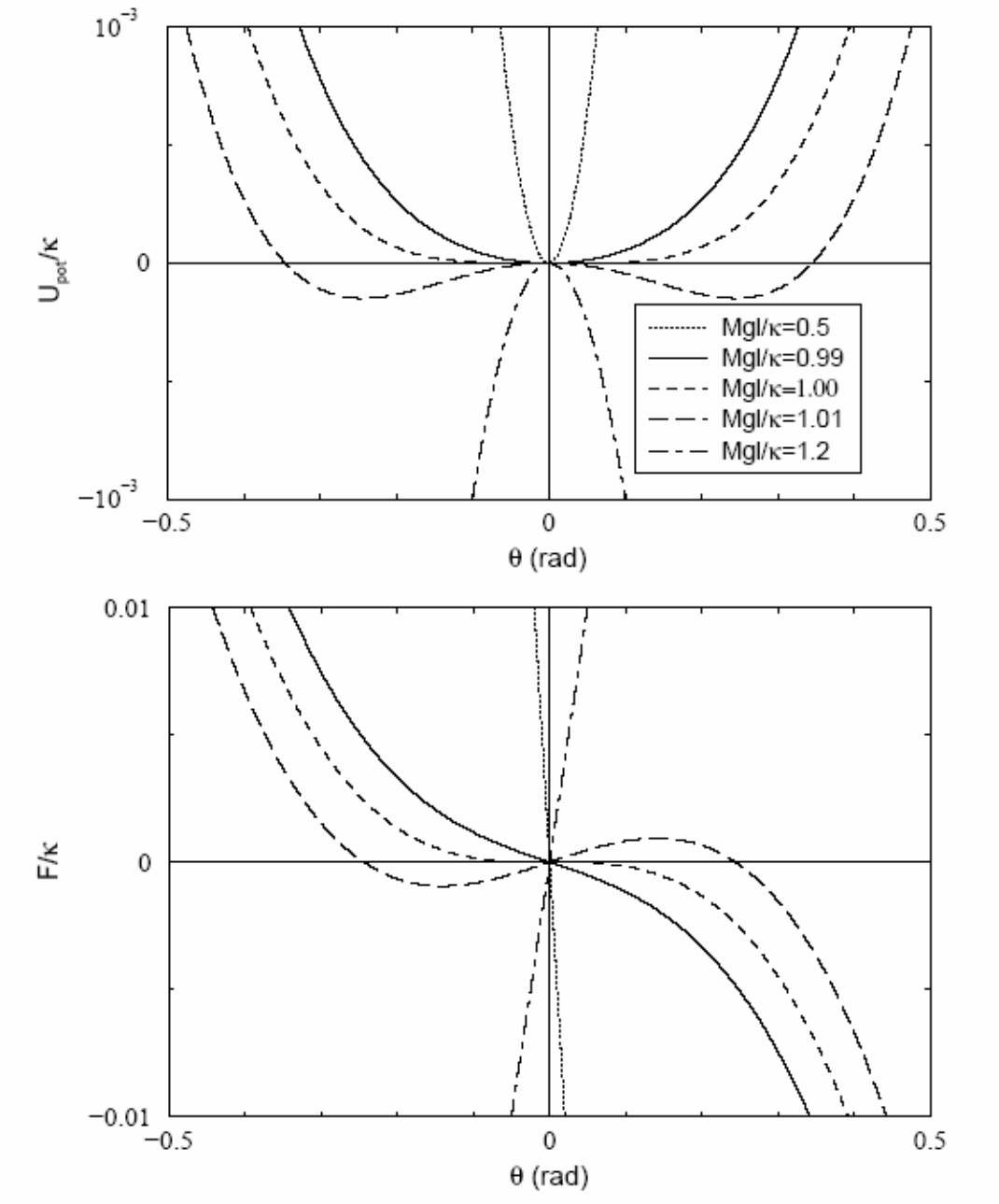

Figure 2.2: Reduced potential energy Upot/k is plotted for different values of the gravity-elastic ratio $R = Mgl/k$

When $\tilde{k} \approx 0$ the system is an oscillator with resonant frequency:

$$f_0 = \frac{1}{2\pi}\sqrt{\frac{k}{M} - \frac{g}{l}} \tag{2.7}$$

In principle, by properly tuning the spring stiffness and the suspended load one can obtain an arbitrarily small resonant frequency. Actually, in the real mechanical system, the frequency cannot be made arbitrarily small while still preserving the stability of the inverted pendulum. The target frequency of 30 mHz seems to be an achievable compromise between the attenuation performance and the need of a safe stability margin.

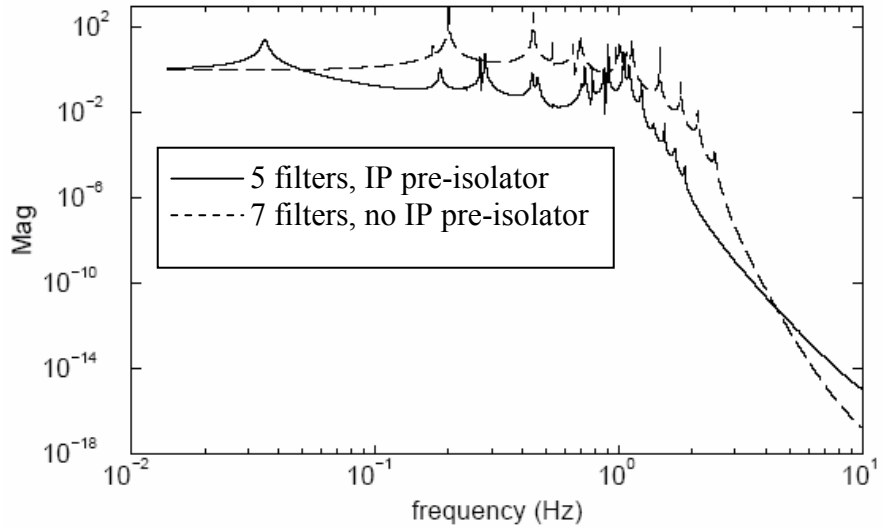

Figure 2.3: Calculated transfer function for an attenuator with 7 filters and no pre-isolator (former design) and the new SA with 5 filters and the pre-isolator stage (IP and filter 0)

Figure 2.3 shows the effect of the inverted pendulum on the attenuation performance of the Super Attenuator: it introduces a double pole in the transfer function at 30 mHz, thus providing $1/f^2$ pre-attenuation starting at its resonance frequency. The lower the IP frequency the more visible is the pre-isolation effect.

2.2 Theory of the Inverted Pendulum

To better understand the details of IP motion (see Figure 2.4) we write down the lagrangian *L* of the IP, including the effect of the rod mass and moment of inertia.

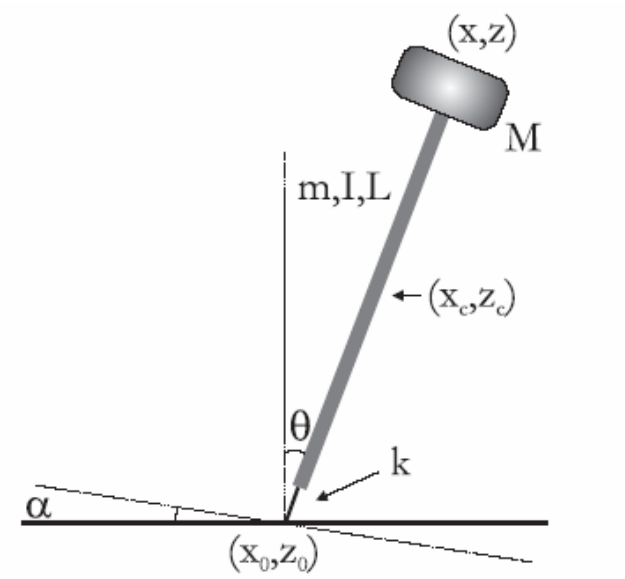

Figure 2.4 Schematic model of the inverted pendulum

We also consider the effect of the seismic tilt of the ground: let $\alpha(t)$ be the angle of the soil with respect to the horizontal axis as a function of the time. Let us name m the leg mass and J its moment of inertia with respect to its centre of mass (*c.o.m.*) C. Let (x, z) be the coordinates of the suspended mass (top of IP), (x_c, z_c) the coordinates of the leg c.o.m., x_0 the horizontal coordinate of the suspension point, the soil tilt with respect to x axis, θ the leg angular displacement with respect to *z* axis. Let *k* be the linear stiffness of the elastic joint (defined so as to provide a restoring force $F_{el} = -k \cdot \delta x$ when the top is displaced by an amount δx). We neglect the vertical seismic motion, which is completely transmitted to the top up to very high frequencies and then attenuated by the first filter of the cascade.

The lagrangian is:

$$\mathcal{L} = \frac{1}{2}M\dot{x}^2 + \frac{1}{2}m\dot{x_c}^2 + \frac{1}{2}J\dot{\theta}^2 - Mgz - mgz_c - \frac{1}{2}kl^2\left(\theta - \alpha(t)\right)^2 \qquad (2.8)$$

For a uniform leg and for small oscillations we can write:

$$
\begin{aligned}
x_c &= \frac{1}{2}(x + x_0) \\
z_c &\simeq \frac{l}{2}(1 - \frac{1}{2}\theta^2) \\
z &\simeq l(1 - \frac{1}{2}\theta^2) \\
\theta &\simeq \frac{x - x_0}{l}
\end{aligned}
$$

Eq. (2.8) thus becomes:

$$
\begin{aligned}
\mathcal{L} &= \frac{1}{2}M\dot{x}^2 + \frac{1}{8}m(\dot{x} + \dot{x}_0)^2 + \frac{1}{2}\frac{J}{L^2}(\dot{x} - \dot{x}_0)^2 + \\
&+ \frac{1}{2}\frac{g}{l}\left[M + \frac{m}{2}\right](x - x_0)^2 - \frac{1}{2}k\,(x - x_0 - l\alpha)^2
\end{aligned}
\tag{2.9}
$$

2.2.1 Equation of horizontal motion

The equation of motion is obtained from

$$
\frac{\mathrm{d}}{\mathrm{d}t}\frac{\partial \mathcal{L}}{\partial \dot{x}} - \frac{\partial \mathcal{L}}{\partial x} = 0 \tag{2.10}
$$

yielding:

$$
\left[M + \frac{m}{4} + \frac{J}{l^2}\right]\ddot{x} + \left[\frac{m}{4} - \frac{J}{l^2}\right]\ddot{x}_0 - \frac{g}{l}\left[M + \frac{m}{2}\right](x - x_0) + k(x - x_0 - l\alpha) = 0 \tag{2.11}
$$

Equation (2.11) is immediately solved in the frequency domain[1]:

$$
x(\omega) = \frac{1}{[\omega_0^2 - \omega^2]}\left\{[\omega_0^2 + \beta\omega^2]x_0(\omega) + y\alpha\right\} \tag{2.12}
$$

Where:

[1] Letting $x(t) = \frac{1}{2\pi}\int_{-\infty}^{\infty} X(\omega)e^{j\omega t}d\omega$

$$\omega_0^2 = \frac{k-(M+\frac{m}{2})\frac{g}{l}}{M+\frac{m}{4}+\frac{J}{l^2}} \tag{2.13}$$

$$\beta = \frac{\frac{m}{4}-\frac{J}{l^2}}{M+\frac{m}{4}+\frac{J}{l^2}} \tag{2.14}$$

$$y = \frac{kl}{M+\frac{m}{4}+\frac{J}{l^2}} \tag{2.15}$$

Treating the leg as a uniform beam (below its own resonant frequency) one has:

$$J = \frac{1}{12}ml^2 \tag{2.16}$$

and the previous equations simplify as follows:

$$\omega_0^2 = \frac{k-(M+\frac{m}{2})\frac{g}{l}}{M+\frac{m}{3}} = \frac{k-A}{D} \tag{2.17}$$

$$\beta = \frac{\frac{m}{6}}{M+\frac{m}{3}} = \frac{C}{D} \tag{2.18}$$

$$y = \frac{kl}{M+\frac{m}{3}} = \frac{kl}{D} \tag{2.19}$$

To plot the transfer function (2.12) one has to eliminate the singularity at $\omega = \omega_0$, keeping into account the dissipation in the system. The main source of dissipation is internal friction, which can be described by replacing the stiffness *k* with the complex stiffness:

$$k \to k(1+i\phi(\omega)) \tag{2.20}$$

The loss angle $\phi(\omega)$ can be assumed to be constant $\phi(\omega)=\phi$ over a wide range of frequencies and its value depends on the material. Then in (2.12), (2.17) and the (2.19) must be replaced by the new expressions:

$$\begin{cases} \omega_0 \to \omega_0 + i(\phi k/D) \\ y \to y(1+i\phi) \end{cases} \tag{2.21}$$

2.3 The centre of percussion effect

Equation (2.12) is, in some way, surprising: at frequencies $f >> f_0/\sqrt{\beta}$, the (spectral) motion of the rod top is:

$$x(\omega) \approx -\beta x_0(\omega) \tag{2.22}$$

There is a critical frequency $f_c = f_0/\sqrt{\beta}$ above which the transfer function flattens and the IP does not behave as an attenuator anymore [6]. Including the effects of dissipation and neglecting the effect of tilt eq. (2.12) is written:

$$\frac{x(\omega)}{x_0(\omega)} = \frac{\omega_0^2 + \beta\omega^2 + i(k\phi/D)}{\omega_0^2 - \omega^2 + i(k\phi/D)} \tag{2.23}$$

In Figure 2.5 the transfer function (2.23) is calculated using the actual values of the parameters foreseen for the IP final design and plotted for 3 different values of β. The presence of the $\beta\omega^2$ term in (2.12) is associated to the *center of percussion effect*: when the base of the leg is shaken by translation seism at "high" frequencies ($\omega >> \omega_0/\sqrt{\beta}$), the leg rotates around a "center of percussion" which remains still. Therefore, the leg top countershakes of an amount depending on β (as shown in eq. (2.22)).

From (2.22) it appears that for the correct operation of the IP superattenuator stage, it is necessary to make $\beta = 0$ or small enough to push the critical frequency beyond all other superattenuator resonances ($f_c \geq 5Hz$). This is equivalent to push the percussion point toward $s = l$, that is to make P to coincide with the suspension point of the load, or with the hinge point of the elastic joint.

To make $\beta = 0$ there are essentially three ways:

- to have massless legs ($m = 0$, $\beta = 0$) : unfeasible, but it is still useful to design legs as light as possible;
- to suspend the top table at the level of the percussion point: this would require an heavy leg segment sticking above the top table;
- to provide the legs with a counterweight below the elastic joint to move the percussion

point near the hinging point of the flexible joint.

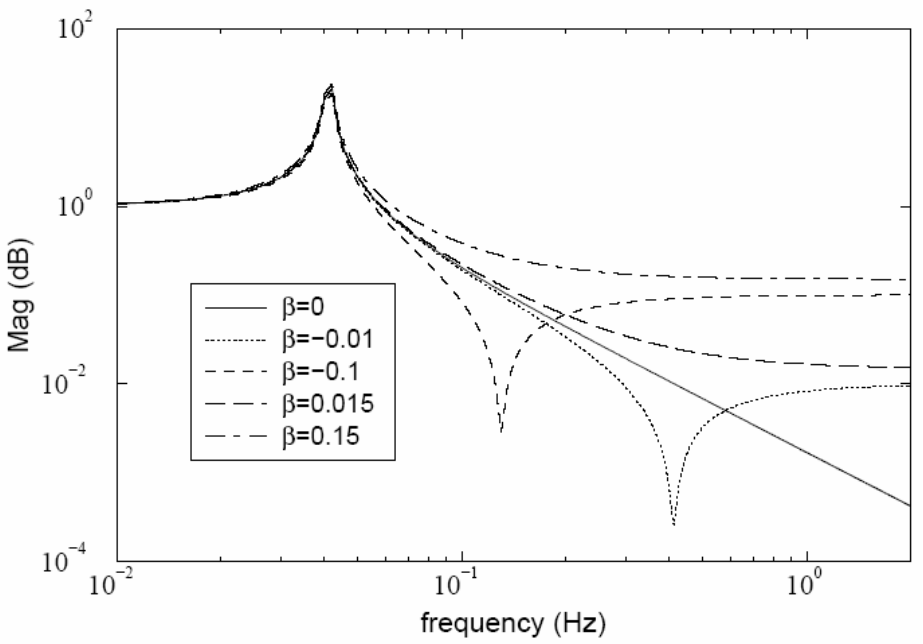

Figure 2.5: Inverted pendulum transfer function (2.23) calculated for different values of β: when $\beta = 0$ the transfer function is that of an ideal pendulum (no centre of percussion effect). When $\beta > 0$ the centre of percussion effect turns into a flattening of the transfer function. When $\beta < 0$, a dip is present, above which the transfer function flattens.

2.3.1 Implementation

The technical solution adopted is to have light aluminum legs and fit them with a counterweight below the elastic joint. The position of the percussion point along the leg depends on the mass and the position of the counterweight, which both can be used to make *P* coincide with the desired position.

The new IP is shown in Figure 2.6: the counterweight is fixed below the IP point by means of a bell shaped structure. We define the following design parameters:

- masses: m_1 (load mass), m_2 (leg mass), m_3 (bell mass), m_4 (counterweight mass);
- lengths: l_1 (leg length), $l_2 = l_1/2$ (distance of leg centre of mass from the suspension point);

We assume momenta of inertia: $J_1 = J_4 = 0$ (the load and the counterweight are considered as point masses), $J_{2,3} = m_{2,3} l_{1,4}^2 / 12$ (the leg and the beam are considered as thin rods).

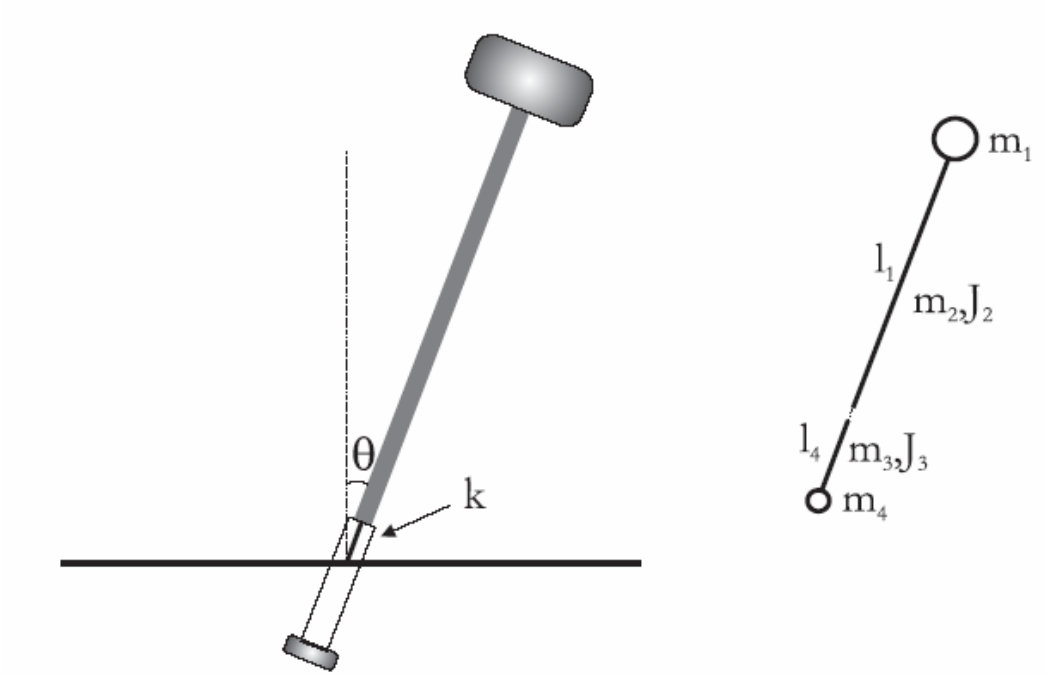

Figure 2.6: Schematic model of the inverted pendulum provided with a counterweight. Beside, the notation used in the calculation is shown.

3. Finite element analysis: Ansys

Ansys is a general purpose finite element modeling package [7]. In general, a finite element solution may be broken into the following three stages:

1. Preprocessing: define the problem through the following major steps:
    - Define key points/lines/areas/volumes
    - Define element type and material/geometric properties
    - Mesh lines/areas/volumes as required

The amount of detail required (i.e. the meshing and related computational burden) will depend on the dimensionality of the analysis (i.e. 1D, 2D, axi-symmetric, 3D).

2. Solving:

- Specify the loads (localized or distributed), the contraints (translational and rotational), finally solve the resulting set of equations.

3. Postprocessing: further processing and viewing of the results; in this stage one may e.g. wish to see:
    - Lists of nodal displacements
    - Forces and torques
    - Deflection plots
    - Stress contour diagrams

3.1 Inverted Pendulum

Inverted pendulum, of which a picture is shown in Figure 3.1 a, is a structure composed of several elements. I designed it in each detail using Solid Works® tool, as shown in Figure 3.1 b, starting from the drawings shown in Figure 3.2 [9].

Figure 3.1 a: Prototype of IP

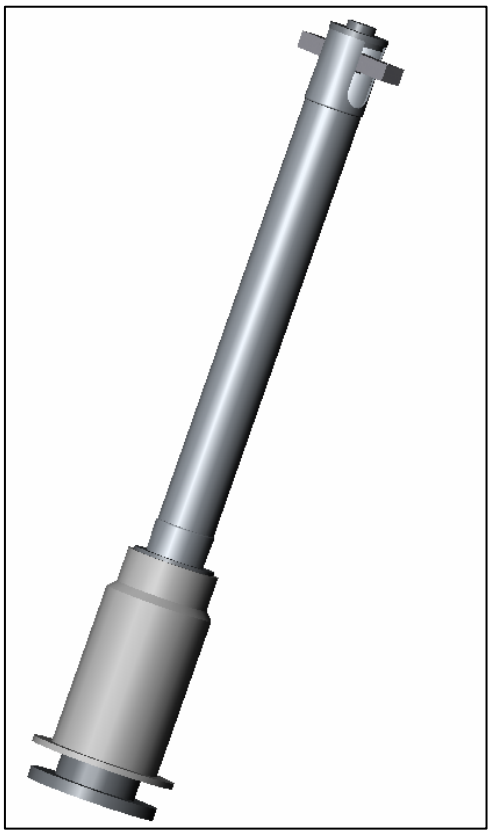

Figure 3.1 b: IP drawn in Solid Works

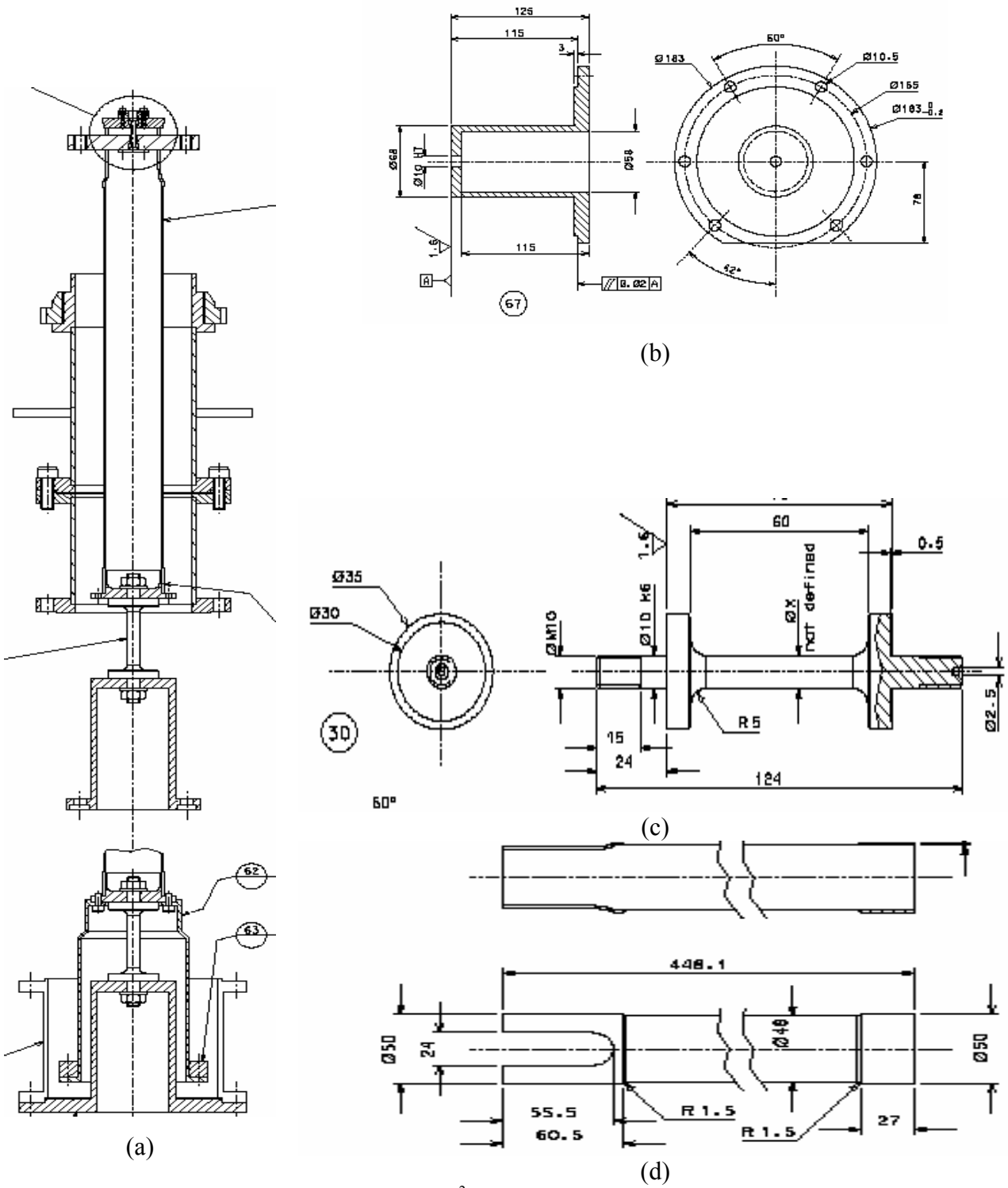

Figure 3.2: Drawings of the Inverted Pendulum[2]; (a) IP; (b) flex joint base; (c) small flex joint; (d) leg

[2] All HAM-SAS drawings are available from the LIGO DCC data base www.lio.caltech.edu/DCC with the drawings numbers ranging from 051100 to 051200

The most important elements of IP, for the purpose of simulation, can be reduced to: 2 flex joints (the small one and the main), counter weight bell (the bell where counter weight is mounted) and leg. The parameters of these components affect significantly the results. The table on the top of the system is made of aluminium, is 40 mm thick, and is weighting 357 Kg. In the following table the relevant parameters of the main elements mentioned above are reported.

Name of element	Length (mm)	Diameter (mm)	Material	Modulus of elasticity
IP leg	448.1	50	EN6082	70 GPa
Main flex joint	76	10	Maraging	190 GPa
Counterweight bell	125	68	AISI 304	193 GPa
Small flex joint	30	3	Maraging	190 GPa

Table 3.1: Values of a few components of IP

In Ansys® I further assigned the material properties of each part of the IP. The first operation was the meshing, as shown in Figure 3.3, as usual in every finite element code.

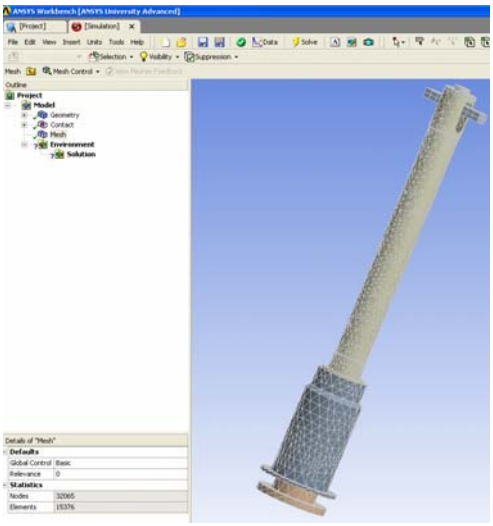

Figure 3.3: Meshing of the IP

The convergence test, shown in Figure 3.4, was made to check that the simulation finds stable resonance frequencies. I changed the mesh in a range between 300 and 20000 elements for each of the 6 normal mode that Ansys found.

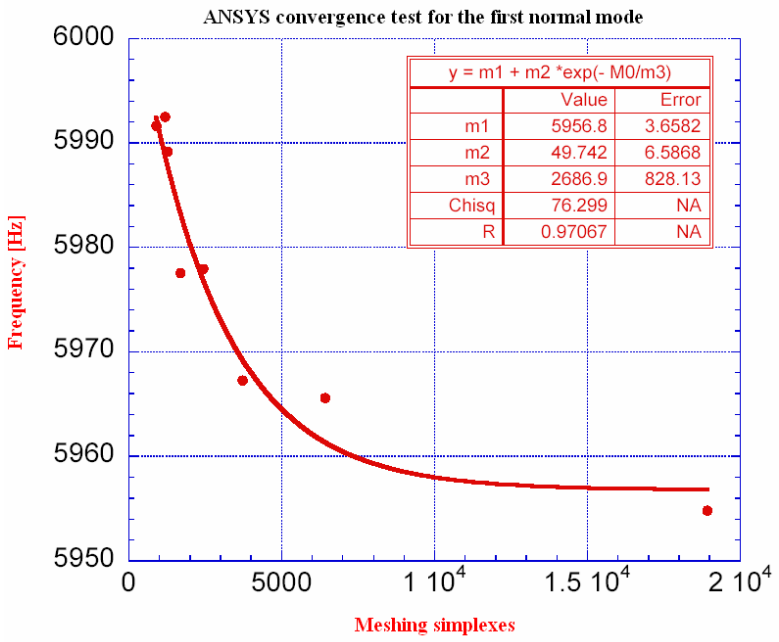

Figure 3.4: Ansys convergence test for the first normal mode

The next step was to simulate the complete isolation stage. I assembled four legs of the IP on two tables in Solid Works: one on the top of the flex joint base and another in the bottom, as shown in Figure 3.5.

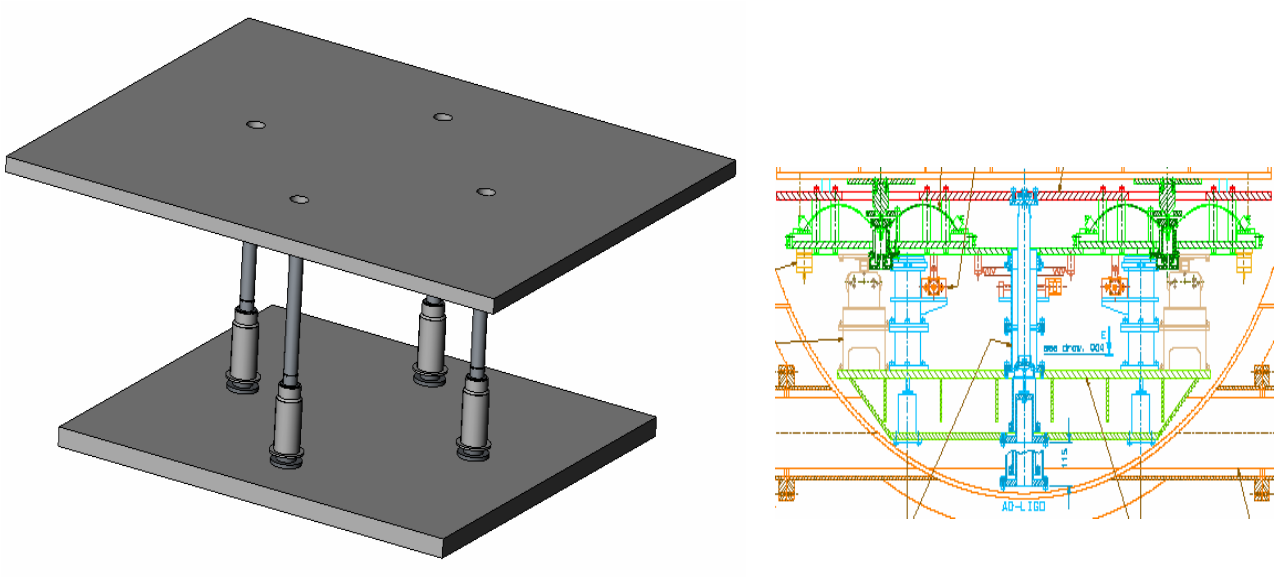

(a) (b)

Figure 3.5: (a) Complete isolation stage; (b) corresponding drawing

I imported it to Ansys where I applied the "Standard Earth Gravity" model, I chose the boundary conditions. Ansys was able to solve the model, analyzing the first 20 modes (see Figure 3.6).

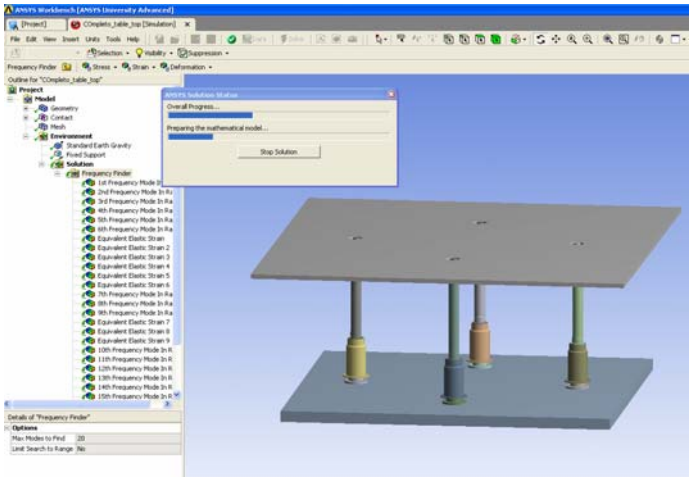

Figure 3.6: Ansys window for SAS simulation

4. Results

Ansys found 20 modes; the first 3 are "**table normal modes"** and concern the motion of the table in order of increasing frequency: the first is the yaw motion, the second the longitudinal motion and the third is the transversal motion (see Figure 4.1).

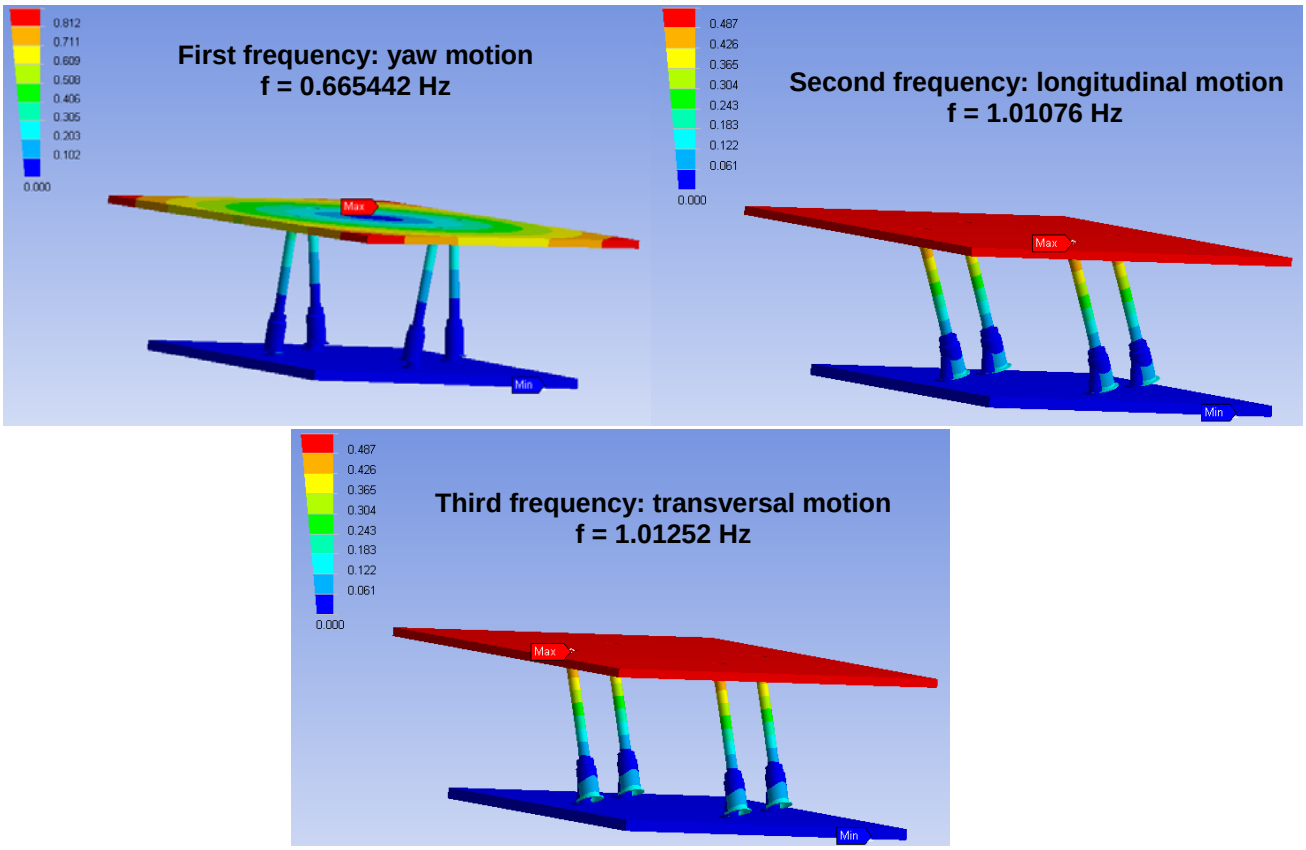

Figure 4.1: Table normal modes: (a) yaw motion; (b) longitudinal motion; (c) transversal motion

I changed the mass of the table on the top in a range between 300 Kg and 1100Kg. I choose as maximum value 1100 Kg because it's the limit that the table can admit

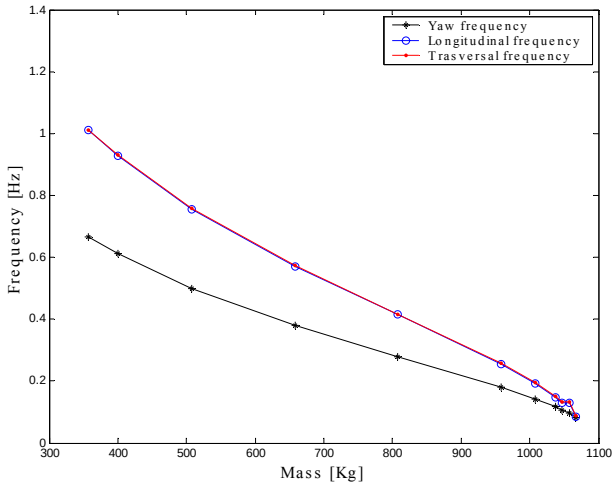

Figure 4.2: Mass vs frequency

According to theory (Equation 2.7) frequency decreased with increasing of the mass (see Figure 4.2). The longitudinal and the transversal motion remain almost unchanged and

the zero-frequency point is the same for all the 3 main modes. The results obtained by measurement on a prototype [8], shown in Figure 4.3, and those found by Ansys are compared in Figure 4.4. Ansys results are fully validated by the measurement results, which proves the validity of the model.

Figure 4.3: Prototype attenuation system

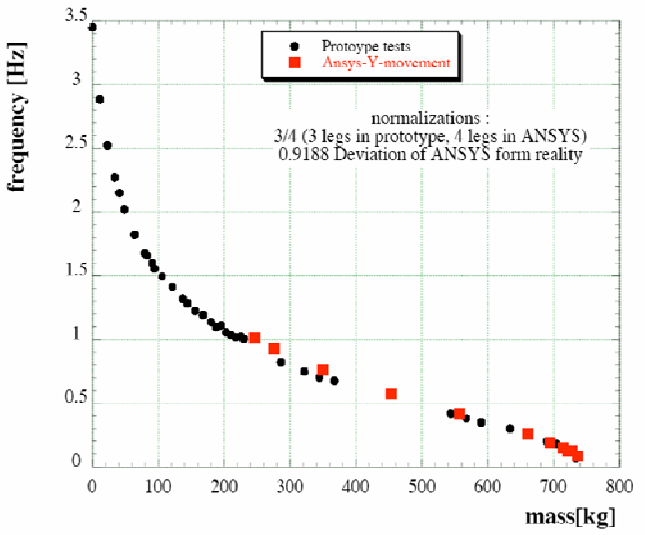

Figure 4.4: Validation of results

From eleventh mode to eighteenth there are the "**rigid leg resonances**", so called because the leg is not stressed, as shown in Figure 4.5 d. The main flex joint presents a "C-stress", the small one a "S-stress", so called because of the shapes of two joints (see Figure 4.5 b and 4.5 c). There are 8 such modes because each leg has 2 (degenerate) modes, in fact they're free to move around the main flex joint. Ansys results show that for a system build with 1.5 mm diameter small flex-joints, without counterweight bell (1.212 Kg), the resonance frequency for the first of these 8 modes is 122 Hz; measurement on the prototype gave 103 Hz, resulting into a discrepancy of 20%. Adding a counter weight bell didn't reduce significantly the resonant frequency, which decreased to 110.6 Hz. This resonance could be damped using eddy-current dampers: the damping times can be thus reduced by a factor of the order of 100, as shown in Figures 4.6 a and b.

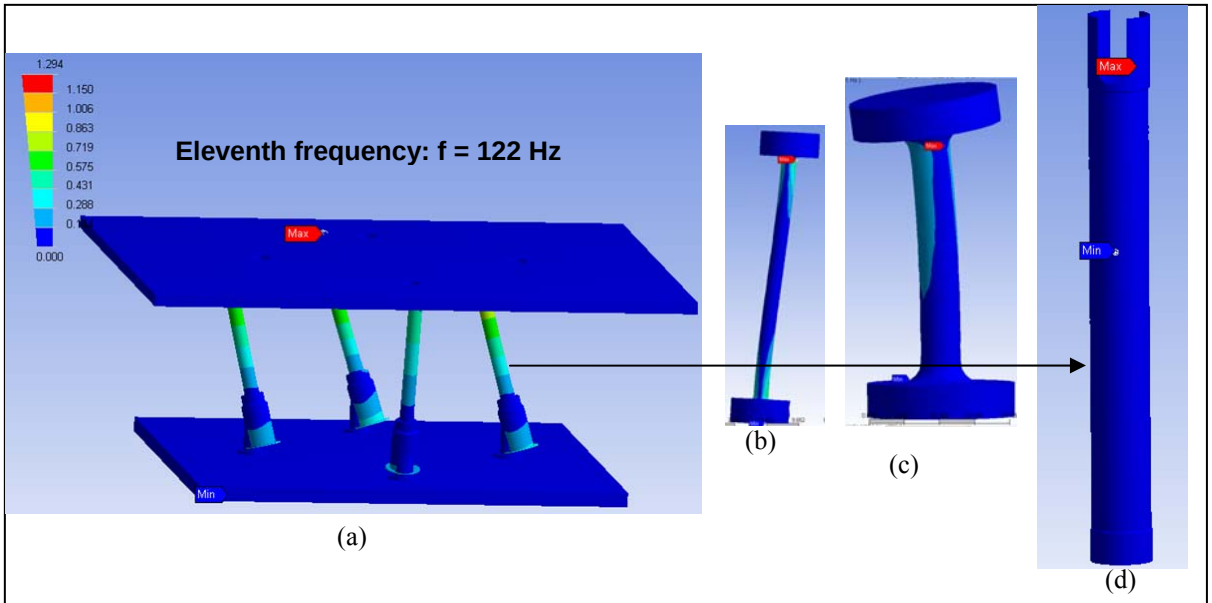

Figure 4.5: Rigid leg resonances (a) Table; (b) small flex joint: S-stress; (c) main flex joint: C-stress; (d) leg

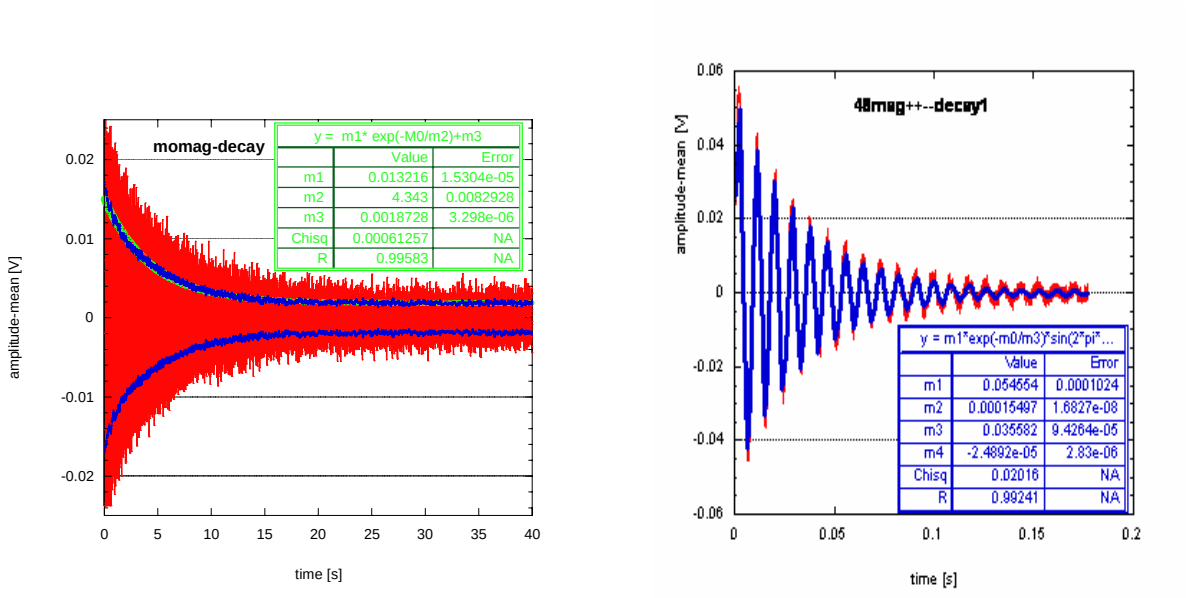

Figure 4.6: Effect of Eddy current dampers (a) before installation, (b) after installation

For a system build with 3 mm diameter small flex-joints, without counterweight bell, the resonance frequency is 235.3 Hz, adding a counter weight bell it decreases to 178.3 Hz; these results are shown in Table 4.1.

	Resonance frequency with counterweight	Resonance frequency without counterweight
Diameter of small flex-joint: 1.5 mm	~110.6 Hz	~122 Hz
Diameter of small flex-joint: 3 mm	~178.3 Hz	~235.3 Hz

Table 4.1: Rigid leg resonances

Modes from nineteenth to twenty-sixth are the "**banana resonances**", so called because of the shape of the leg, as shown in Figure 4.7. In this modes not only the 2 flex joints are stressed but also the leg. The frequencies are higher and these resonances move the head of the legs, so damping will be even more effective.

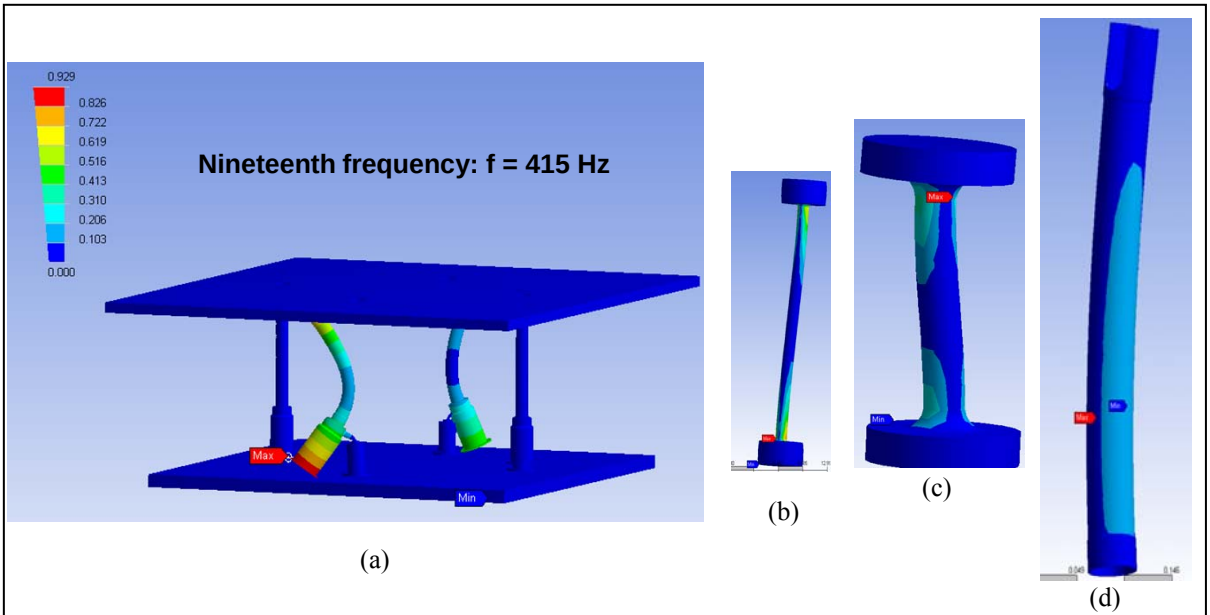

Figure 4.7: Banana resonances (a) Table; (b) small flex joint; (c) main flex joint; (d) leg

For a system build with 1.5 mm diameter small flex-joints, without counterweight bell, the resonance frequency for the first of these 8 modes is 415 Hz, adding a counter weight bell it decreases to 210.6 Hz; using 3 mm diameter small flex-joints, without counterweight bell, the

resonance frequency is 424 Hz, adding a counter weight bell it decreases to 253.3 Hz; these results are shown in Table 4.2.

	Resonance frequency with counterweight	Resonance frequency without counterweight
Diameter of small flex-joint: 1.5 mm	~210.6 Hz	~415 Hz
Diameter of small flex-joint: 3 mm	~253.3 Hz	~424Hz

Table 4.2: Banana resonances

The fourth, fifth and sixth resonances are "**spring box resonances**" (see Figure 4.8). The only dangerous one is the pitch motion, but the problem can be mitigated with magnetic dampers; if those are not enough, extra resonant dampers may be required

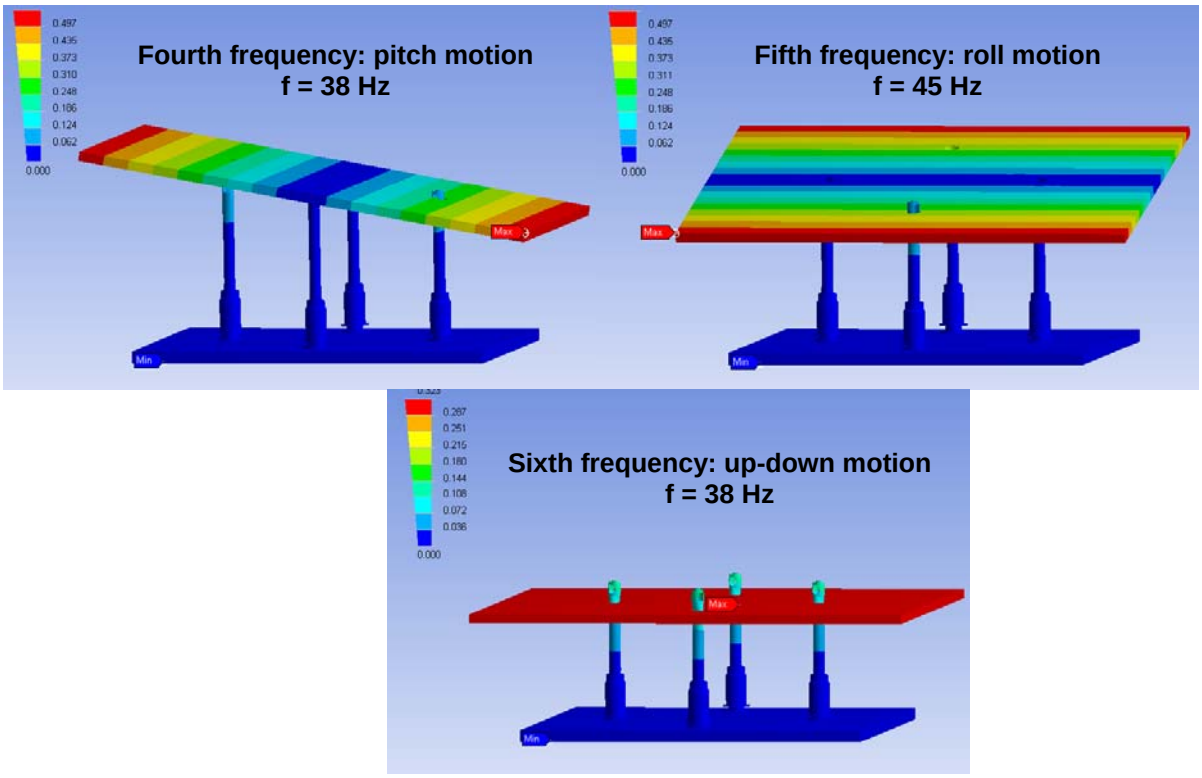

Figure 4.8: Spring box resonances: (a) pitch motion; (b) roll motion; (c) up-down motion

5. Future steps

Next step will be to characterize the dynamic behavior of SAS in terms of transfer function(s) between the top and the bottom tables motions.

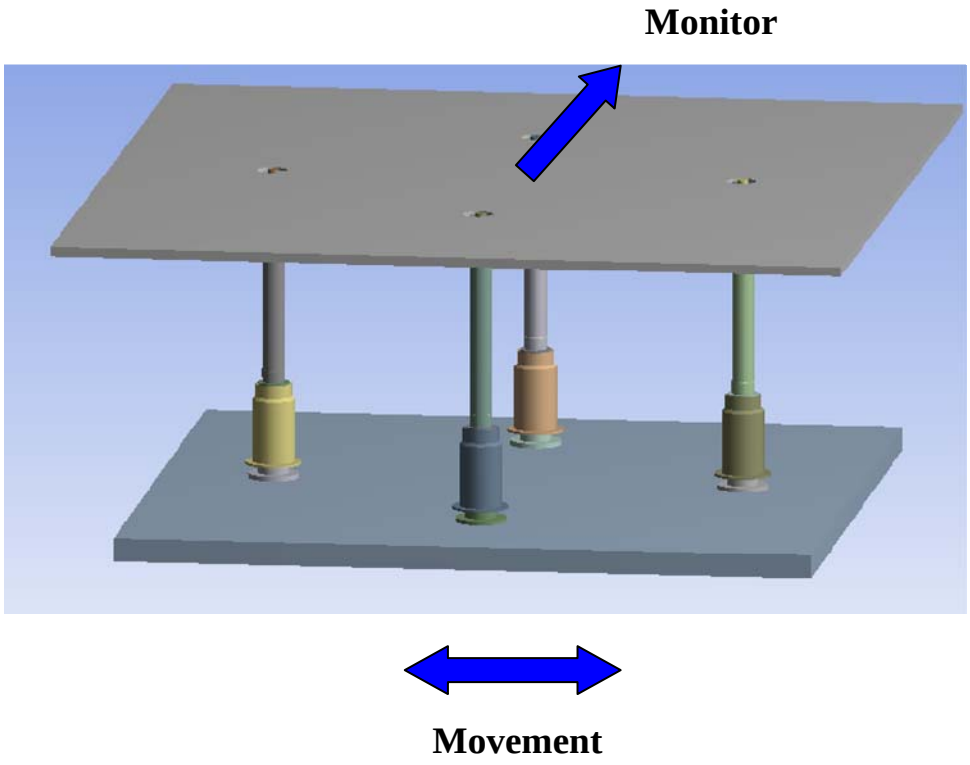

Figure 5.1: Representation of the transfer function

From a design viewpoint, the aim is to determine a counter weight that effectively neutralizes the percussion point effects. Prototype measurements indicate that the transfer function saturates at 80 dB without counterweight. A proper counter weight should allow 100 dB attenuation, which is the design goal.

6. Acknowledgments

First of all, I would like to thank Professor Innocenzo M. Pinto for the unique opportunity he gave me to do research at Caltech, and for his support. I'd like to thank my supervisor at CalTech, Dr. Riccardo De Salvo and my mentor, Dr. Calum I. Torrie, for the support and helpful guidance throughout the 10 weeks I spent at Caltech and for their encouragements and patience. Thanks to Juri Agresti and Virginio Sannibale for invaluable help. I'd like to thanks, besides, the friends I made at CalTech: they made this summer unforgettable.

References

[1] R. Hulse and J. Taylor, "Discovery of a pulsar in a binary system", *The Astrophysical Journal*, vol 195 pp.L51-L53, 1975.

[2] P.R. Saulson, *Phys. Rev. D*, vol. 42 N.10, pp 2437-2439, 1990.

[3] A. Takamori, "Low Frequency Seismic Isolation for Gravitational Wave Detectors", Ph.D dissertation, LIGO Project, University of Tokyo, 2002.

[4] A. Rohay, "Ambient Ground Vibration Measurements at the Livingston", Louisiana LIGO Site, LIGO Project C961022-A-D, 1996.

[5] F. Raab and D. Coyne "Effect of Microseismic Noise on a LIGO Interferometer", LIGO Project T960187-01-D, 1997.

[6] G.Lo Surdo, "Ultra Low-Frequency Inverted Pendulum for the VIRGO Test Mass Suspension", Ph.D dissertation, Scuola Normale Superiore di Pisa, 1998.

[7] University of Alberta Ansys Tutorial: http://www.mece.ualberta.ca/tutorials/ansys/index.html

[8] R.De Salvo, C.Galli, G.Gennaro, M.Mantovani, S.Marka, V.Sannibale, A.Takamori, C.Torrie, A.Bertolini, "Passive Seismic Attenuation for the LIGO Output Mode Cleaner", proceedings of Amaldi-6 at Okinawa, 2005, to be published in Classical Quantum Gravity.

CONTENTS